NASA
Technical
Paper
2395

April 1985

In-Flight Surface Oil-Flow Photographs With Comparisons to Pressure Distribution and Boundary-Layer Data

Robert R. Meyer, Jr.,
and Lisa A. Jennett

NASA

NASA Technical Paper 2395

1985

In-Flight Surface Oil-Flow Photographs With Comparisons to Pressure Distribution and Boundary-Layer Data

Robert R. Meyer, Jr.,
and Lisa A. Jennett

Ames Research Center
Dryden Flight Research Facility
Edwards, California

National Aeronautics
and Space Administration

Scientific and Technical Information Branch

SUMMARY

Oil-flow photographs were interpreted, with regard to chord location of shocks, relative shock strength, and chord location of boundary-layer transition, and were compared to results obtained from pressure distributions and boundary-layer measurements. The investigation was conducted in flight at transonic speeds on an F-111 transonic aircraft technology (TACT) aircraft, which had been fitted with a natural laminar-flow airfoil test section.

Results of the comparison indicated that the location and strength of shock waves, as well as laminar, transition, and turbulent flow, can be accurately determined from in-flight oil photographs. It was also noted that the presence of oil on the airfoil test section did not significantly affect the pressure distribution measurements or transition location.

INTRODUCTION

It is often desirable to document flow phenomena by means of flow visualization. The visualization of flow can clarify such aerodynamic phenomena as where shock waves occur and whether flows are laminar, turbulent, or separated. As a result of the need for flow visualization, certain techniques have been developed in association with various test facilities. In wind tunnels, for example, Schlieren photography (ref. 1), oil flows (ref. 2), and tufts (ref. 3) are used extensively. Water tunnels use dye for flow visualization (ref. 4). Tufts, sublimation of chemicals (ref. 5), and oil (refs. 6 and 7) have been used in flight for flow visualization.

During the summer of 1980, NASA Ames Research Center's Dryden Flight Research Facility (DFRF) conducted an investigation to determine the amount of natural laminar flow that could be achieved in flight on a supercritical airfoil at transonic speeds. The investigation was conducted on an F-111 transonic aircraft technology (TACT) aircraft (ref. 8) which had a portion of the wing modified with a natural laminar-flow (NLF) airfoil section. As part of the NLF study, pressure distributions and boundary-layer measurements, along with upper surface oil flows, were obtained. The oil flows were part of a "piggyback" experiment attendant to the NLF investigation and, therefore, are somewhat limited.

In this paper, oil-flow results are presented and interpreted with regard to the chord location of shocks, relative shock strength, and chord location of boundary-layer transition. The interpretation of the oil-flow photographs is supplemented by chordwise pressure distribution data and aft-chord boundary-layer-thickness data. The oil mixture used and method of application are discussed briefly, as are the observed effects of the oil on the pressure distributions and the boundary-layer results. Data are presented for Mach numbers from 0.81 to 0.85 and wing sweep angles of 9°, 16°, and 25°.

NOMENCLATURE

$\mathfrak{L}$	center line
C_p	pressure coefficient, $p - p_\infty/q$
c	local wing chord
h_p	pressure altitude
M	free-stream Mach number
NLF	natural laminar flow
PD	pressure distribution
PD_{fg}	pressure distribution, favorable gradient

PD_{ug}	pressure distribution, unfavorable gradient
p	local static pressure
p_∞	free-stream static pressure
q	free-stream dynamic pressure, $0.7M^2p_\infty$
SAE	Society of Automotive Engineers
TACT	transonic aircraft technology
x	chordwise distance from the leading edge
z/c	ratio of vertical distance of airfoil to local wing chord
α	corrected angle of attack, deg
Δ	incremental change
δ	boundary-layer thickness, cm(in)
Λ	wing sweep, deg

TEST AIRCRAFT AND INSTRUMENTATION

F-111 TACT Natural Laminar Flow

An NLF supercritical airfoil was fitted over a portion of the wing panels of the F-111 TACT aircraft. The F-111 TACT aircraft is described in reference 8, and the airfoil sections installed on the aircraft are shown in figure 1. The right wing glove was the test section while the left wing glove served primarily to maintain aircraft symmetry, minimizing changes in aircraft flying qualities. The foam and fiberglass techniques discussed in reference 9 were used to construct the airfoil test section.

The partial-span glove enveloped the F-111 TACT wing between 56- and 75-percent semispan at a wing sweep of 10°. The airfoil was installed with the chord lines streamwise at a wing sweep of 10°. Airfoil coordinates, surface finish, and surface waviness limits for the test section were 0.025 cm (0.010 in), 250 μm, and 0.005 cm (0.0002 in) per 2.54 cm (1 in), respectively. For the NLF airfoil tests, leading- and trailing-edge flaps were locked in an undeflected position, and all but the outboard spoilers were deactivated. Because of the addition of the gloved region, wing sweep was limited to between 9° and 43° for these tests. Oil-flow test data were obtained at 9°, 16°, and 25° wing sweep. The aircraft was limited to a maximum Mach number of 0.85, maximum dynamic pressure of 20.3 kPa (425 lb/ft^2), and a maximum normal acceleration of 2g for these NLF tests.

Instrumentation

The right wing partial-span glove was instrumented with a chordwise row of flush static pressure orifices on the centerline of the glove's upper and lower surfaces. The upper and lower surface rows consisted of 15 orifice locations each. Upper and lower surface boundary-layer rakes (fig. 2) were located at 90 percent of the test section chord. Only the upper surface data are presented in this paper, since oil photographs were obtained on that surface only. Differential pressure transducers, located in the wing bays and referenced to a common absolute pressure source, were used to make pressure measurements from the flush orifices and the boundary-layer rakes. The absolute pressure source was in the wing box near the fuselage and was fed into a reference tank in the fuselage.

Reference data, such as Mach number, altitude, angle of attack, and angle of sideslip, were obtained from an aircraft noseboom system. An uncompensated pitot-static probe was used for reference air-data measurement. In-flight airspeed calibration data were used to correct indicated values of Mach number, static pressure, and altitude. Flow direction vanes were mounted on the noseboom to

determine angle of attack and angle of sideslip. Angle of attack was adjusted for upwash and fuselage bending.

CONFIGURATIONS AND PROCEDURES

Natural Transition

Pressure distributions and boundary-layer measurements were obtained, with the test section kept as clean and smooth as possible to prevent premature boundary-layer transition from laminar to turbulent. These flights were made to document the natural transition characteristics of the test section with and without oil.

Forced Transition

For some of the test flights, transition strips were installed on the test section for successive flights at 5-, 20-, 30-, 40-, and 50-percent chord in an effort to calibrate boundary-layer thickness as a function of established transition location. The transition strips consisted of Carborundum[1] grains on the airfoil surface from the inboard to the outboard edge of the test section. The grain size used was scaled by the method of reference 10 to produce enough surface roughness to trip the boundary layer from laminar to turbulent; however, the grains were not large enough to cause drag themselves. The grain size used for transition strips forward of 40-percent chord was 0.297 mm to 0.350 mm (0.0117 in to 0.0138 in) in diameter. Since the laminar boundary layer becomes thicker farther aft and is able to withstand more surface roughness, a grain size of 0.350 mm to 0.419 mm (0.0138 in to 0.0165 in) in diameter was used at 40-percent chord and aft. The strips were bonded with a plastic adhesive to clear tape that had been previously attached to the test section.

[1]Carborundum Co., Niagara Falls, N.Y.

Flow Visualization Procedure

The flow visualization medium chosen for this investigation was Society of Automotive Engineers (SAE) 80-W-90 oil mixed with powdered black graphite in proportions of four parts of oil to one part of graphite, by volume. This particular mixture was chosen for three reasons:

1. This weight of oil was believed to be thick enough to remain in place during the warm temperatures of takeoff and climbout, yet be thin enough to flow on the test section at the colder temperatures of altitude.

2. This weight of oil was readily available.

3. The black graphite and oil mixture would provide contrast against the white test section.

The mixture was applied to the surface with a paintbrush approximately 30 min prior to takeoff. The test aircraft climbed to the first test point immediately after takeoff. Each test condition was held for approximately 2 min to allow the patterns in the oil to become established before photographs were taken from the chase aircraft. To aid in the interpretation of the photographs, constant chord lines were drawn across the test section at 10 percent intervals.

During the oil-flow test, flight conditions with the highest wing sweeps (which were assumed to be the most forward transition) were normally flown first. The reasoning for this procedure is presented in greater detail in the Oil Performance section of this report.

The oil technique was used only at altitudes equal to or less than 7.6 km (25,000 ft) after it was discovered that at higher altitudes the oil became too thick to flow with ease on the airfoil test section.

Oil Performance

As previously mentioned, oil used in flight for flow visualization must be able to remain on the test section during takeoff and climbout, yet flow on the test section at altitudes representative of the relatively cold temperatures and at transonic velocities. For this experiment, the oil became too thick to flow at altitudes between 7.6 km and 9.1 km (25,000 ft to 30,000 ft). The thickening of the oil at high altitudes is attributed to the reduced temperatures at altitude, which causes an increase in the viscosity of the oil. Figure 3 shows temperature as a function of altitude from weather balloon data for the day of flight. At 7.6 km to 9.1 km (25,000 ft to 30,000 ft) the free-stream temperature was about -9.5° C to -20.5° C (15° F to -5° F). Therefore, it appears that the particular oil mixture used is useful to temperatures down to a free-stream temperature of -9.5° C to -20.5° C (15° F to -5° F) at Mach 0.8. To obtain data at any lower temperatures, oil or a fluid of different viscosity characteristics would be required.

A potential problem exists using this oil technique for visualization of transition, because oil is not continuously supplied to the leading edge of the test section. As previously noted, test conditions with the highest wing sweep (most forward transition) were flown first. This was done so that oil would be available on the leading edge to visualize the transition to a turbulent boundary layer. For example, if a test condition was flown with transition to a turbulent boundary layer occurring significantly forward of transition on a previous test condition, a minimal amount of oil would be available to visualize the turbulent condition. This could result in an erroneous interpretation of the oil flow. A potential solution would be to supply oil to the leading edge of the test section during flight. However, this approach would require additional hardware and would add complexity to the technique.

Another requirement for oil used as a flow visualization medium is illumination of the oil on the test section. The black graphite, which was mixed with the oil in proportions of 4:1 by volume, produced adequate illumination of the oil when the test section was in sunlight. However, a greater concentration of graphite would have more clearly illuminated the oil mixture. Recent studies at NASA (ref. 11) have shown that ferrous oxide (putty black), mixed in proportions of 15 parts of oil to 1 part of ferrous oxide by volume, works more satisfactorily.

NLF CONCEPTS

The airfoil test section, on which this study was conducted, was based on a concept to achieve a laminar boundary layer over a major portion of the forward region of the airfoil. Because the oil-flow experiment was conducted on this test section, a review of the NLF concepts may aid in the discussion of the results. Shown in figure 4 is the candidate upper surface pressure distribution that was used as a design for the airfoil test section. To sustain a laminar boundary layer for subsonic and transonic conditions, the chordwise pressure gradient ($\Delta c_p/\Delta x/_c$) must remain negative (favorable) over the forward portion of the airfoil. In figure 4, the favorable pressure gradient extends from the leading edge of the airfoil ($x/c = 0$) to almost the 60-percent chord ($x/c = 0.60$). The pressure gradient becomes unfavorable when the C_p values begin to increase along the chord. In figure 4, this occurs just ahead of $x/c = 0.60$. The positive or unfavorable gradient causes an instability in the boundary layer; if the flow has been laminar up to the point of unfavorable gradient, it will undergo transition to a turbulent

boundary layer. However, it should be noted that other sources of instability can cause the boundary layer to transition to a turbulent condition before encountering an unfavorable pressure gradient. Some sources of these instabilities are surface roughness or waviness, leading-edge crossflow, and large chord Reynolds numbers.

PRESENTATION OF RESULTS

The results of this investigation are presented in the following figures:

RESULTS AND DISCUSSION

Oil-Flow Patterns and Pressure Distributions

Figures 5 through 13 present in-flight photographs of the oil-flow patterns and, when available, corresponding pressure distributions. The figures are presented in the order in which the photographs were taken. This allowed "time related" trends in the oil-flow patterns, such as loss of oil on the test section — particularly near the leading edge — to be observed.

Rather than discussing each figure separately, the observations made from the oil-flow photographs and trends noted in the pressure distributions are limited to a few "representative" cases. No discussion of the visualization of separated flow is included in this paper because the low angle-of-attack nature of the NLF tests caused minimal or no separated flow on the NLF test section. However, based on wind tunnel oil-flow experience, the in-flight oil-flow technique would be expected to correctly identify separated flow conditions.

Observation of Shock-Free and Mostly Turbulent Flow

Figure 5 represents a takeoff and climbout condition and is presented as a shock-free and mostly turbulent flow condition for visual reference purposes. No pressure distribution data were available for figure 5.

Observation of Shock Flow

An apparent observation that can be made from most of the oil-flow photographs beginning with figure 6 is a dark,

curved line across the test section just aft of the midchord. This is attributed to a normal shock wave on the test section which causes the oil to build up, or puddle, at the location of the shock. This is verified vividly in figure 7, which presents an oil-flow photograph and pressure distribution at $M = 0.85$ and $\Lambda = 25°$. The dark line in the oil-flow photograph intersects the centerline of the test section (the pressure orifice row) at about 65-percent chord ($x/c = 0.65$), which is consistent with the data presented in the pressure distribution. The pressure distribution shows a rapid increase in pressure (increasing c_p) at the same location ($x/c = 0.65$), which also indicates the presence of a shock wave.

A less obvious case can be observed in the oil-flow photograph of figure 8, where there are several lighter lines in the general region where a shock might be located. It is difficult to determine if the lighter lines are multiple shocks across the test section, or residue oil from previous test conditions. However, it is believed that multiple shocks exist on the test section at the particular flight conditions presented. This opinion is supported by both the pressure distribution of figure 8(a) and the oil-flow photograph of figure 9(b). The pressure distribution of figure 8(a) indicates the existence of at least two identifiable shock waves, one at approximately 55-percent chord ($x/c = 0.55$) and another between the 70-percent to 90-percent chord ($x/c = 0.70$ to 0.90). This is in apparent agreement with the oil-flow photograph that shows evidence of shocks at approximately 60-percent and 75-percent chord and either residue oil or another shock at 82-percent chord. In the oil-flow photograph of figure 9(b) at $M = 0.84$ ($M = 0.01$ more than figure 8(b)), the lines have a similar pattern to those noted in figure 8(b). However, they are more sharply defined (indicating more shock strength) and positioned approximately 10 percent farther aft on the test section; these are expected results of a shock due to a small increase in Mach number.

Observation of Laminar, Transition, and Turbulent Flow

A more subtle observation, which can be made from the oil-flow photographs of figures 5 through 13, is the transition from laminar to turbulent boundary-layer flow. An example of this can be seen in figure 8(b). Note the distinction between a light area forward of the 20-percent chord, where there appears to be little or no oil, and a uniform slightly darkened area aft of the 20-percent chord. The light area is considered to be the region of a laminar boundary layer. This belief is supported by the pressure distribution of figure 8(a) as well as boundary-layer data, which is discussed later. In figure 8(a), a favorable gradient exists from the leading edge ($x/c = 0$) to approximately the 20-percent chord ($x/c = 0.20$), at which point the pressure gradient becomes unfavorable and the boundary layer is likely to transition to turbulent. In the photograph, the dark area aft of the 20-percent chord (including the area aft of the shock) is considered to be the turbulent region.

Two additional subtle observations regarding laminar to turbulent transitions are made from the oil-flow photograph of figure 9:

1. Two small dark wedges, located near the center line of the test section, extend aft from the leading edge to the 25-percent chord.

2. A "clean," but interrupted, white band extends across the test section between the 20-percent and 30-percent chord.

The two dark wedges that extend through the laminar flow region indicate two

instances of localized premature transition of the laminar boundary layer to a turbulent condition. They were probably caused by local disturbances on the leading edge. The clean, white band across the test section is believed, in this case, to be an area where transition from a laminar to a turbulent condition extends for several percent chord, rather than occurring abruptly. This type of region is commonly referred to as a "transition region." This belief is supported by the small magnitude of unfavorable pressure gradient at 20-percent to 30-percent chord in the pressure distribution of figure 9(a).

The observations thus far have been limited to cases where transition was apparently caused by the boundary layer encountering an unfavorable pressure gradient at relatively forward chord locations. Figures 12 and 13 present cases where the upper surface pressure distribution is close to the design case shown in figure 4. The favorable pressure gradient extends quite far aft on the test section, specifically to 70-percent chord in figure 12 and 40-percent chord in figure 13. This extent of favorable pressure gradient provides an opportunity for a corresponding amount of laminar flow. However, due to the large chord Reynolds number associated with the extent of the favorable gradient, the laminar boundary layer would be expected to transition to a turbulent condition before encountering the unfavorable pressure gradient. This is apparently confirmed in the oil-flow photograph of figure 12(b), which indicates the beginning of transition at approximately 25 percent, compared to the beginning of the unfavorable gradient at 70-percent chord in the pressure distribution of figure 12(a).

A detailed analysis of the oil-flow photographs and pressure distributions of figures 5 through 13 (using the techniques and criteria previously described) has been made. The estimated shock location, shock strength, and transition location determined from oil-flow photographs, as well as shock location, shock strength, and unfavorable pressure gradient location determined from pressure distributions, are summarized in table 1 and will be discussed in detail in the following sections.

Effect of Oil on Pressure Distribution

Initially, there was some concern that the presence of oil on the test section would adversely affect the static pressure measurement. Figure 14 presents representative data intended to define the effect of oil on the test section pressure distribution. Specifically, figure 14 compares the pressure distribution with oil on the test section to similar conditions (Mach number (M) and angle of attack (α)) without oil for three wing sweeps. It can be discerned from figure 14 that the oil had a minimal, if any, effect on these measurements.

Determination of Transition Location From Boundary-Layer Thickness

The boundary-layer measurements were used as a primary source for determining the approximate transition location. This was accomplished by measuring the boundary-layer thickness (δ) as a function of angle of attack (α) for various fixed transition locations. This is because a turbulent boundary layer is much thicker than a laminar boundary layer. The comparison of the clean wing results (natural transition) with the "calibration" data (where transition was forced) provided an indication of the extent of laminar flow achieved on the test section. These results then provided an independent method of determining the point of boundary-layer transition for comparison with the results obtained from the oil-flow photographs.

Figures 15(a) to 15(e) present the variation of the upper surface boundary-layer thickness (δ) obtained from boundary-layer rakes as a function of angle of attack. With the use of trip strips, transition was forced on successive flights at 5-, 20-, 30-, 40-, and 50-percent chord on the test section without oil. The lines on the figures represent faired results without oil, and a value of δ (circular symbol) indicates when the oil was on the test section. By referring to the location of this point with respect to the different transition lines, the point of transition can be determined independently of the oil-flow pattern, but concurrent with the oil-flow results. For example, in figure 15(a) ($M = 0.81$ and $\Lambda = 9°$), the "with oil" data point (circular symbol) lies between the 30-percent and 40-percent lines, indicating that transition occurs at about 35-percent chord. A similar analysis was made with the remaining boundary-layer thickness figures; the results are summarized in table 1 and is discussed in detail in the following sections.

Effect of Oil on Boundary-Layer Thickness

Figure 16 presents results of the effect of oil on the test section boundary-layer thickness as determined from the boundary-layer rake data. The case presented is for an unfavorable pressure gradient located at a forward chord location that corresponds to the pressure distribution of figure 7. Although the data points with and without oil for the clean wing were not performed at the exact test conditions (different angle of attack), they both lie very close to the 20-percent chord transition line. The line was obtained from the boundary-layer data when transition was forced at the 20-percent chord. From the comparison, it appears that the presence of the oil did not significantly affect the transition location. In addition to the case presented, it would have been preferable to present a case corresponding to a more demanding criterion (a greater extent of laminar flow); however, the scope of this study did not provide such conditions.

Comparison of Shock and Boundary-Layer Characteristics From Oil-Flow Photographs and Pressure Measurements

Table 1 presents a qualitative summary of results obtained from methods previously discussed. The purpose of the table is to demonstrate the capability of the oil-flow method to "visualize" flow on the upper surface of the test section used for this study. Specifically, shock and boundary-layer characteristics obtained from oil-flow photographs are presented with appropriate pressure measurements for comparison purposes.

Shock Characteristics

Comparison of the shock location and strength results obtained from the oil and pressure distribution (PD) methods show very close agreement, usually within 5-percent chord, and good agreement as to relative strength. The oil-flow method appears to provide a very good visualization of both shock location and strength.

Boundary-Layer Characteristics

The boundary-layer characteristics are divided into three categories: the laminar, the transition, and the turbulent regions. A comparison is made of the laminar and transition regions obtained from the oil to the trends indicated in the pressure distributions, specifically favorable gradient (PD_{fg}) and the unfavorable gradient (PD_{ug}), respectively. These comparisons are made because for most of the cases previously discussed, the laminar boundary layer existed only in the region of a favorable pressure gradient, and transition occurred in the region of the

unfavorable gradient. In the turbulent region, a comparison is made between the transitions determined from oil-flow photographs and from boundary-layer thickness (δ) results. This comparison was made because transition based on boundary-layer thickness results should be an indicator of the beginning of the turbulent boundary layer.

Comparison of the oil-flow analysis, the trends of the pressure distributions, and the boundary-layer thickness analysis shows close agreement, usually within 5-percent chord. Two apparent exceptions are the comparisons of the oil flow and PD results in the laminar and transition regions of figures 12 and 13. In both of these cases, as noted earlier, transition to a turbulent condition occurred ahead of the unfavorable pressure gradient. Because of the far aft location of the unfavorable gradient, the oil and PD trend comparison would not be expected to agree. The oil-flow method used for this study appeared to provide a very good visualization of boundary characteristics, such as laminar flow, transition flow, and turbulent flow.

CONCLUDING REMARKS

An investigation was made regarding the feasibility of using oil for inflight flow visualization on a natural laminar-flow wing. Oil was brushed (painted) on the upper surface of the test section before takeoff. Boundary-layer transition location, shock location, and strength for the upper surface coated with oil are compared to pressure distribution and boundary-layer measurements at similar conditions without oil. The following conclusions and recommendations regarding the use of this oil technique can be made:

1. Location of shock waves can be observed in the oil. These results agreed with those obtained from chordwise surface pressure measurements.

2. Boundary-layer characteristics, such as laminar flow, transition flow, and turbulent flow can be determined from in-flight oil-flow photographs. These results agreed well with trends noted in pressure distributions and results obtained from boundary-layer thickness measurements.

3. The oil has a minimal effect on the pressure distributions or on boundary-layer thickness measurements.

4. The use of oil, applied to the upper surface of a wing prior to takeoff, is a practical and inexpensive technique for in-flight flow visualization.

5. The usefulness of the technique used in this test is limited in altitude because the oil becomes too thick to be of use at colder temperatures of altitude. The limiting altitude, for the Mach number range of these tests, was 7.6 km (25,000 ft).

Ames Research Center
Dryden Flight Research Facility
National Aeronautics and Space Administration
Edwards, California, April 26, 1983

REFERENCES

1. Bracht, K.; and Merzkirch, W.: Schlieren Visualization of the Laminar-to-Turbulent Transition in a Shock-Tube Boundary Layer. AIAA Paper A79-12898, Oct. 1977.

2. Loving, Donald L.; and Katzoff, S.: The Fluorescent-Oil Film Method and Other Techniques for Boundary-Layer Flow Visualization. NASA Memo 3-17-59L, Langley Research Center, 1959.

3. Crowder, James P.: Add Fluorescent Minitufts to the Aerodynamicist's Bag of Tricks. Astronaut. & Aeronaut., Nov. 1980.

4. Lorincz, Dale J.: Flow Visualization Study of the F-14 Fighter Aircraft Configuration. NASA CR-163098, 1980.

5. McTigue, John G.; Overton, John D.; and Petty, Gilbert, Jr.: Two Techniques for Detecting Boundary-Layer Transition in Flight at Supersonic Speeds and at Altitudes Above 20,000 Feet. NASA TN D-18, 1959.

6. Johnson, Harold I.; and Mungall, Robert G.: A Preliminary Flight Investigation of an Oil-Flow Technique for Air-Flow Visualization. NACA RM L54G14a, 1954.

7. Bisgood, P. L.: The Application of a Surface Flow-Visualization Technique In Flight. A.R.C.R.& M. 3769, 1974.

8. Painter, Weneth D.; and Caw, Lawrence J.: Design and Physical Characteristics of the Transonic Aircraft Technology (TACT) Research Aircraft. NASA TM-56048, 1979.

9. Bohn-Meyer, M.; and Jiran, Fred: The Use of Techniques to Modify Airfoils and Fairings on Aircraft Using Foam and Fiberglass. AIAA Paper 81-2445, Nov. 1981.

10. Braslow, Albert L.; and Knox, Eugene C.: Simplified Method for Determination of Critical Height of Distributed Roughness Particles for Boundary-Layer Transition at Mach Numbers from 0 to 5. NACA TN 4363, 1958.

11. Curry, Robert E.; Meyer, Robert R., Jr.; and O'Connor, Maureen: The Use of Oil for In-Flight Flow Visualization. NASA TM-84915, 1984.

TABLE 1. - CHORD LOCATION OF FLOW PHENOMENA

			Shock		Boundary layer					
			Location and strength		Laminar		Transition		Turbulent	
Figure	Λ, deg	Flight condition	Oil at $\mathfrak{L}$, percent	PD, percent	Oil at $\mathfrak{L}$, percent	PD_{fg}, percent	Oil at $\mathfrak{L}$, percent	PD_{ug}, percent	Oil at $\mathfrak{L}$, percent	δ results, percent
4	25	Climb	No shock	---	0 to 14	---	14	---	14 to 100	---
5	25	M = 0.84 α = 4.8°	[a]Weak at 55	[a]Weak at 55 to 60	0 to 16	0 to 15	16	15 to 20	16 to 100	---
6	25	M = 0.85 α = 4.7°	[b]Moderate at 65	[b]Moderate at 65	0 to 20	0 to 15	20	15 to 20	20 to 100	~15
7	16	M = 0.83 α = 4.9°	[a]Weak at 55 [a]Weak at 75 Either shock or residue at 82	[b]Moderate at 55 Possible shock between 70 and 90	0 to 20	0 to 20	20 to 23	20 to 30	23 to 100	20 to 25
8	16	M = 0.84 α = 4.9°	[b]Moderate at 60 [a]Weak at 65	[b]Moderate at 65	0 to 22	0 to 20	22 to 27	20 to 30	27 to 100	---
9	9	M = 0.81 α = 4.8°	[a]Weak at 65 and 75	[a]Weak at 65	0 to 24	0 to 20	24 to 30	20 to 30	30 to 100	35
10	9	M = 0.82 α = 4.8°	[c]Strong at 76	[c]Strong at 70 to 80	0 to 24	0 to 20	24 to 32	20 to 30	32 to 100	30
11	9	M = 0.83 α = 5.0°	[c]Strong at 80	[c]Strong at 70 to 80	0 to 25	0 to 70	25 to 33	70	33 to 100	40
12	25	M = 0.85 α = 4.1°	[a]Possible weak at 60 [a]Weak at 80	[a]Weak at 60 [a]Possible weak at 70 to 90	0 to 25	0 to 40	25 to 35	40 to 50	36 to 100	---

[a]Weak shock, ΔC_p = 0.15 to 0.25.

[b]Moderate shock, ΔC_p = 0.25 to 0.30.

[c]Strong shock, $\Delta C_p \geqslant 0.30$.

ECN 12859

(a) F-111 TACT aircraft with NLF airfoil installed on wing panels.

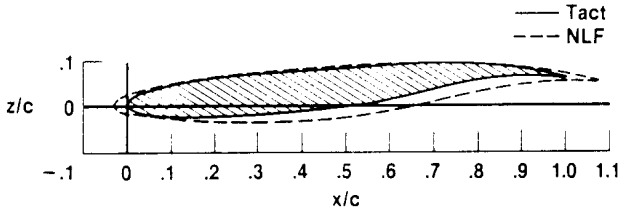

(b) Comparison of NLF and TACT airfoil profiles.

Figure 1. In-flight photograph and airfoil section.

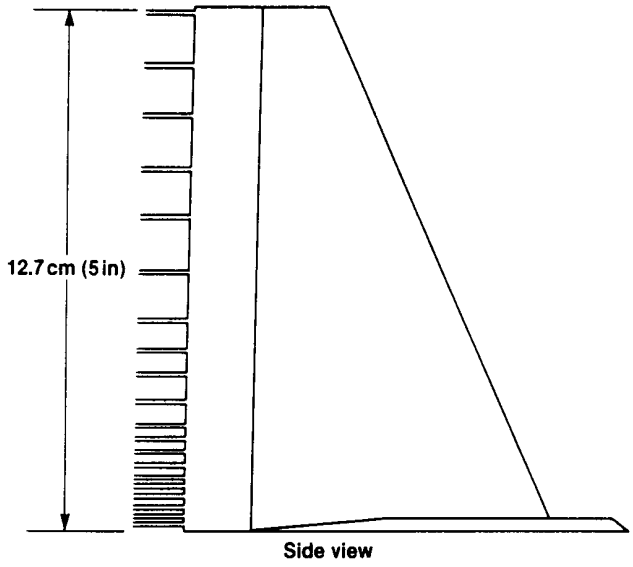

Figure 2. Boundary-layer rake.

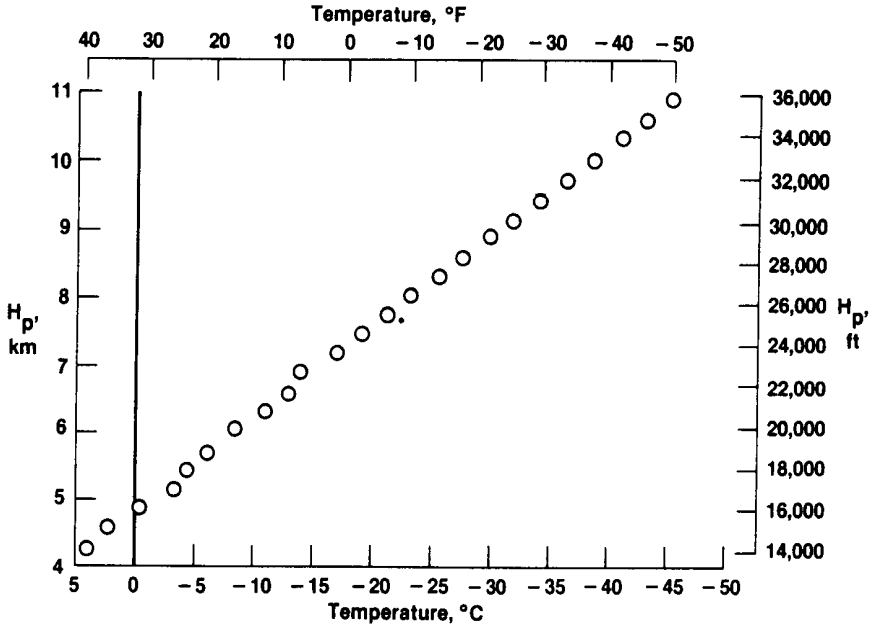

Figure 3. Variation of temperature with altitude.

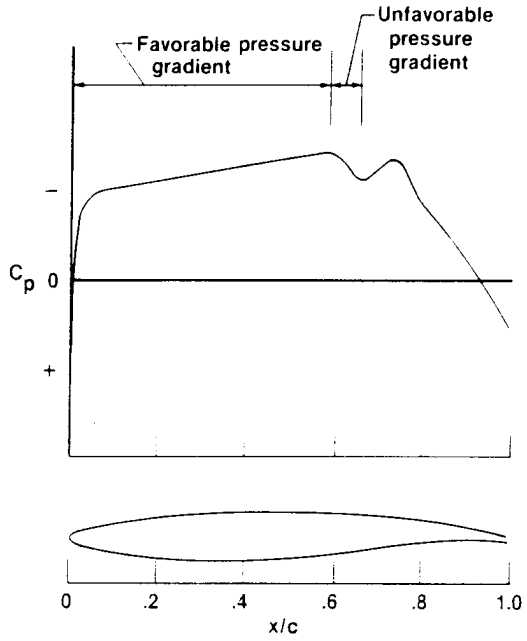

Figure 4. NLF airfoil and design upper surface pressure distribution.

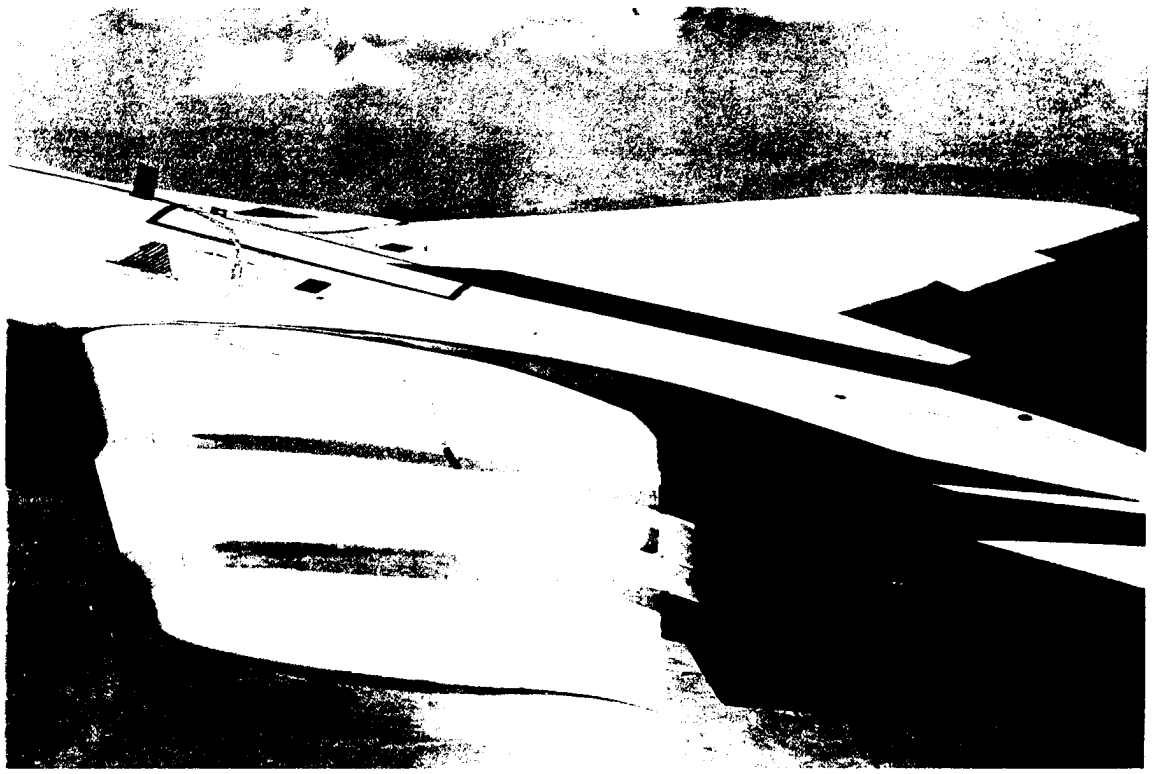

ECN 13414

Figure 5. In-flight photograph of oil on airfoil test section at climb conditions (subsonic and shock free) of approximately 300 knots indicated airspeed and $\Lambda = 25°$.

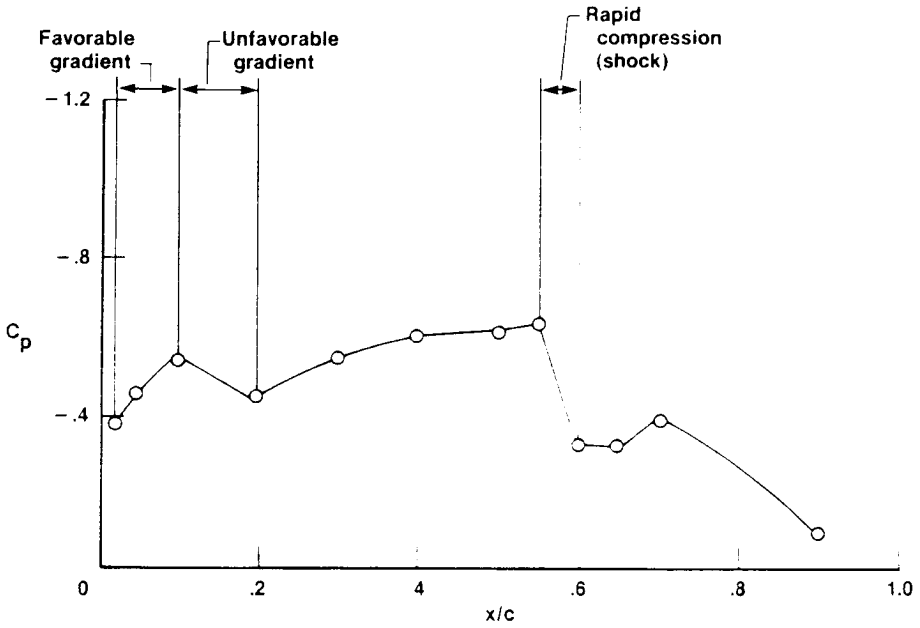

(a) Pressure distribution for flight data with oil.

ECN 13415

(b) Test section with oil.

Figure 6. In-flight oil-flow photograph and upper surface pressure distribution on airfoil test section at M = 0.84, α = 4.8°, and Λ = 25°.

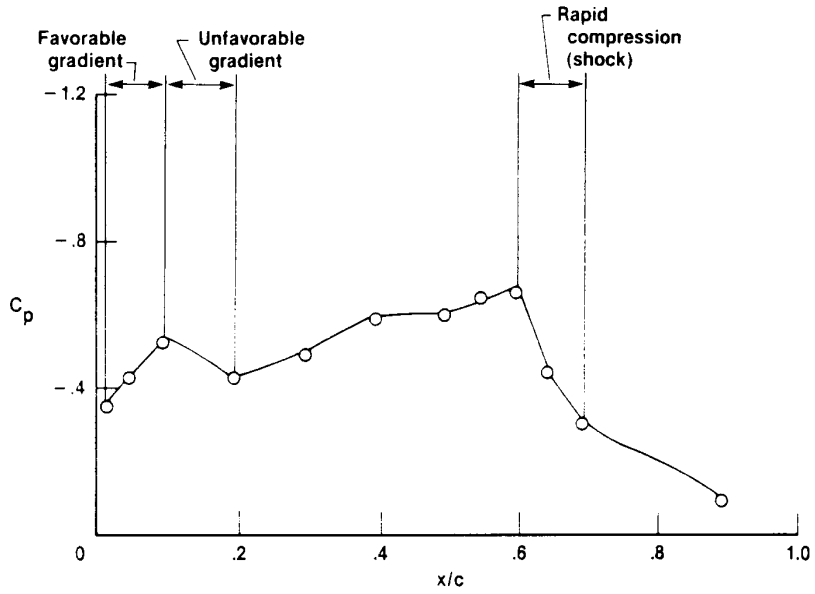

(a) Pressure distribution for flight data with oil.

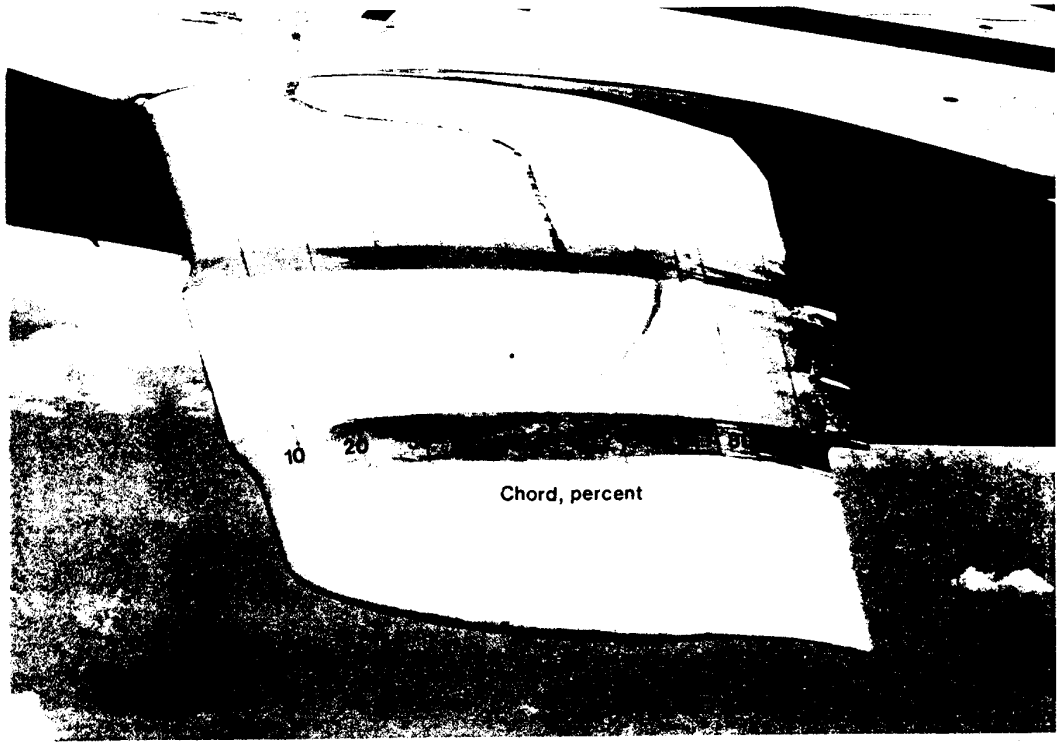

ECN 13418

(b) Test section with oil.

Figure 7. In-flight oil-flow photograph and upper surface pressure distribution on airfoil test section at M = 0.85, α = 4.7°, and Λ = 25°.

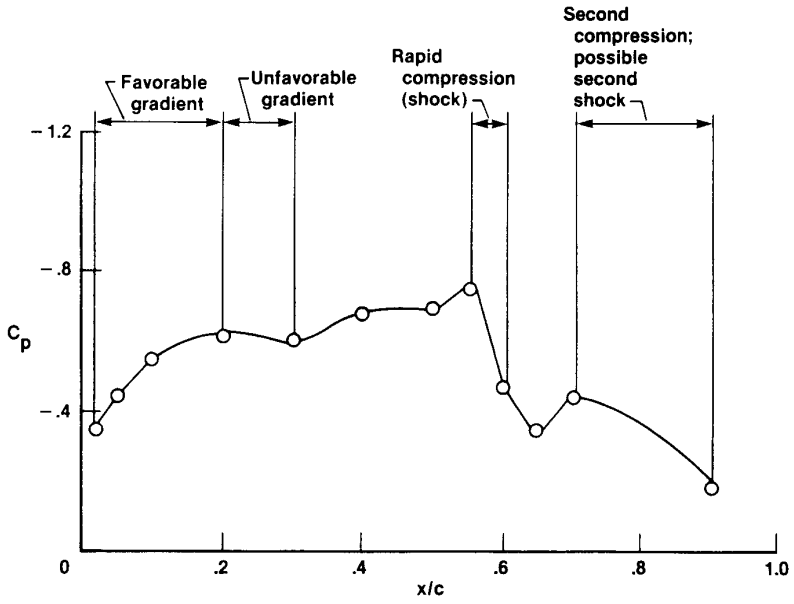

(a) Pressure distribution for flight data with oil.

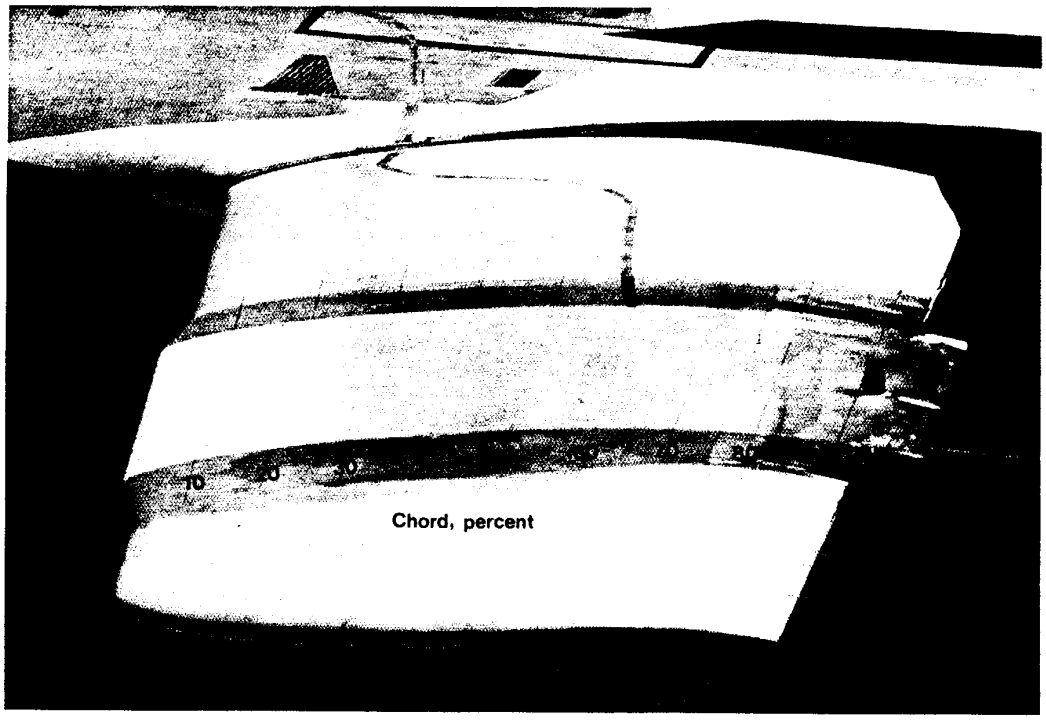

ECN 13419

(b) Test section with oil.

Figure 8. In-flight oil-flow photograph and upper surface pressure distribution on airfoil test section at M = 0.83, α = 4.9°, and Λ = 16°.

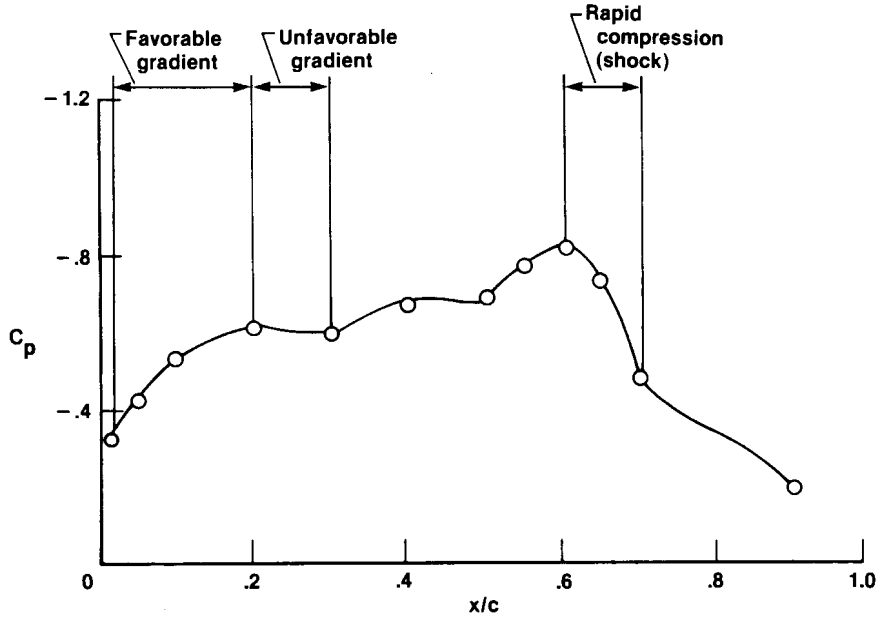

(a) Pressure distribution for flight data with oil.

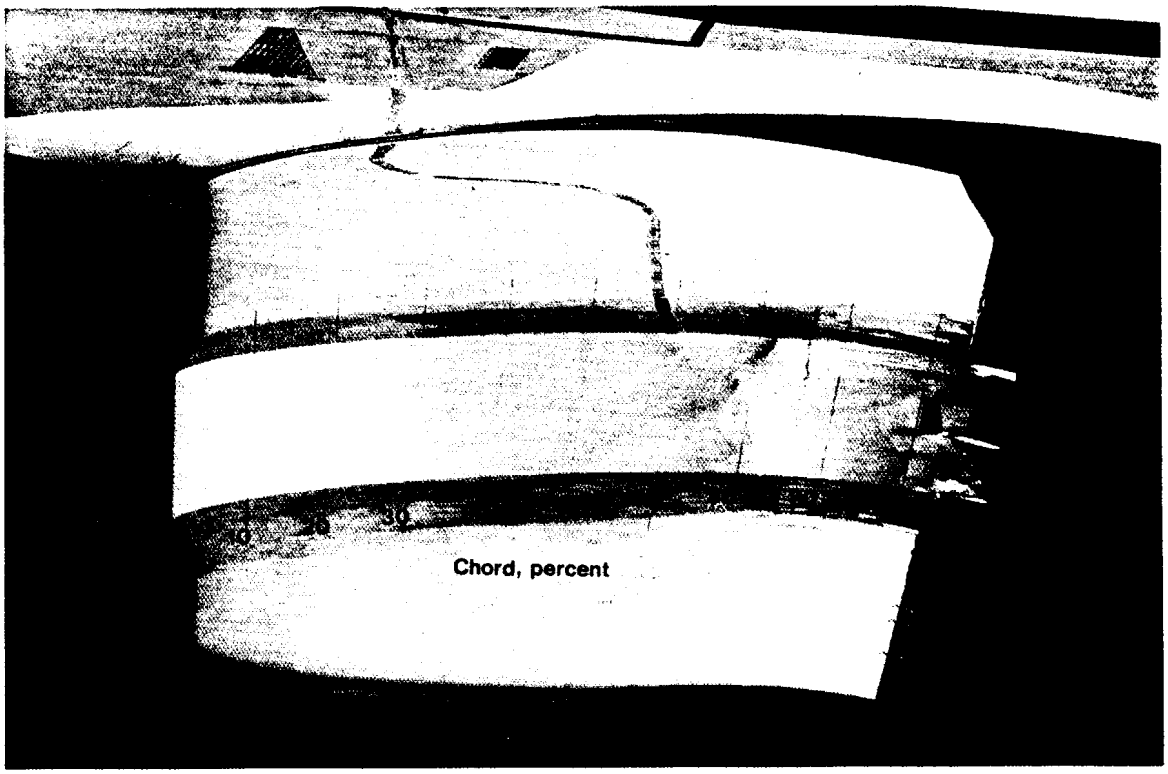

ECN 13421

(b) Test section with oil.

Figure 9. In-flight oil-flow photograph and upper surface pressure distribution on airfoil test section at M = 0.84, α = 4.9°, and Λ = 16°.

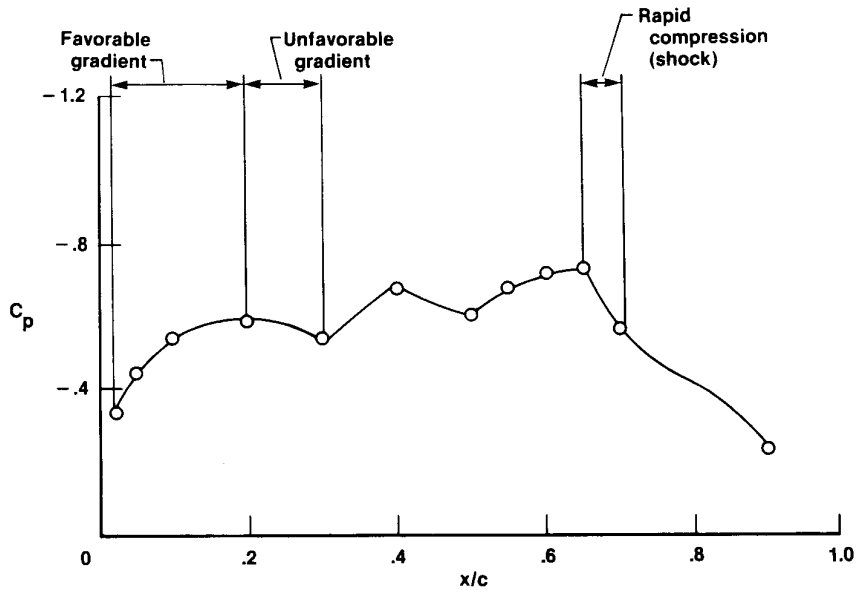

(a) Pressure distribution for flight data with oil.

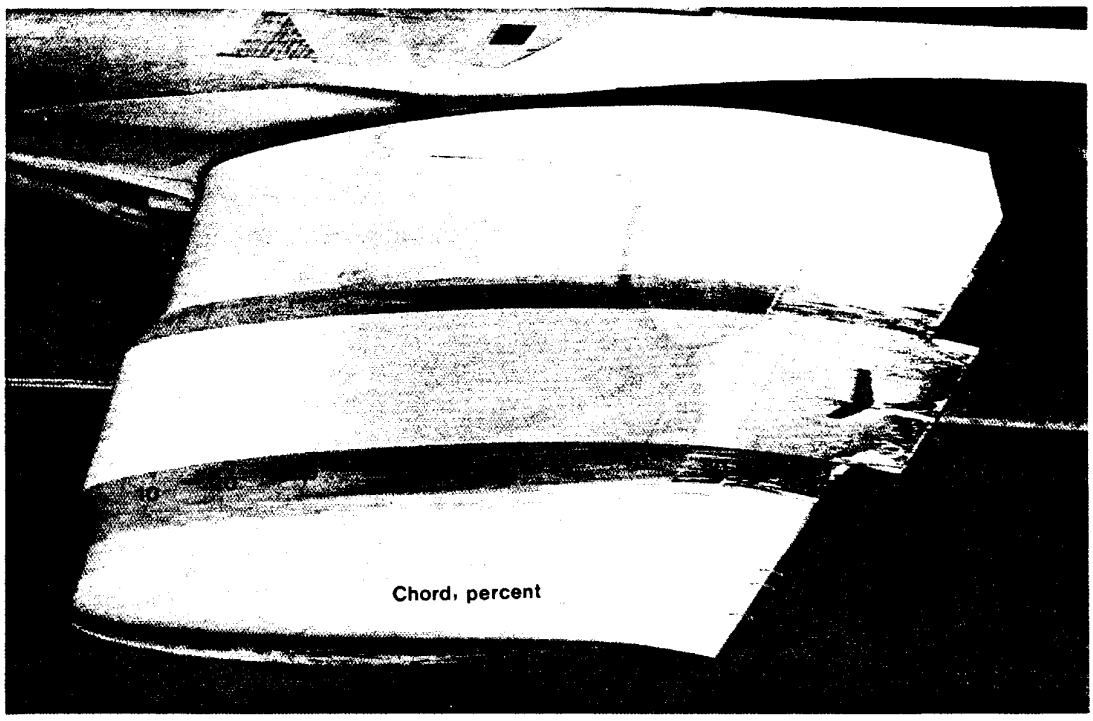

ECN 13423

(b) Test section with oil.

Figure 10. In-flight oil-flow photograph and upper surface pressure distribution on airfoil test section at M = 0.81, α = 4.8°, and Λ = 9°.

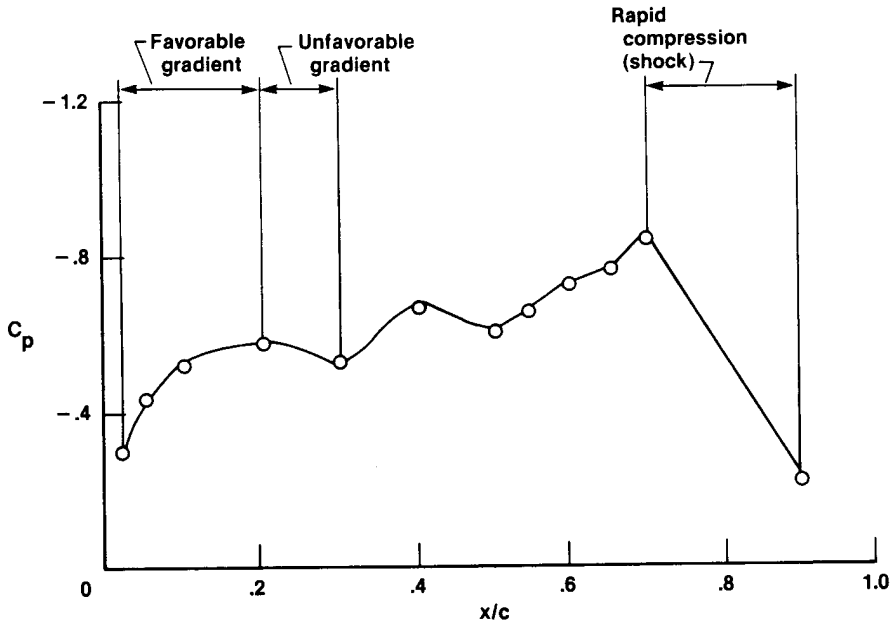

(a) Pressure distribution for flight data with oil.

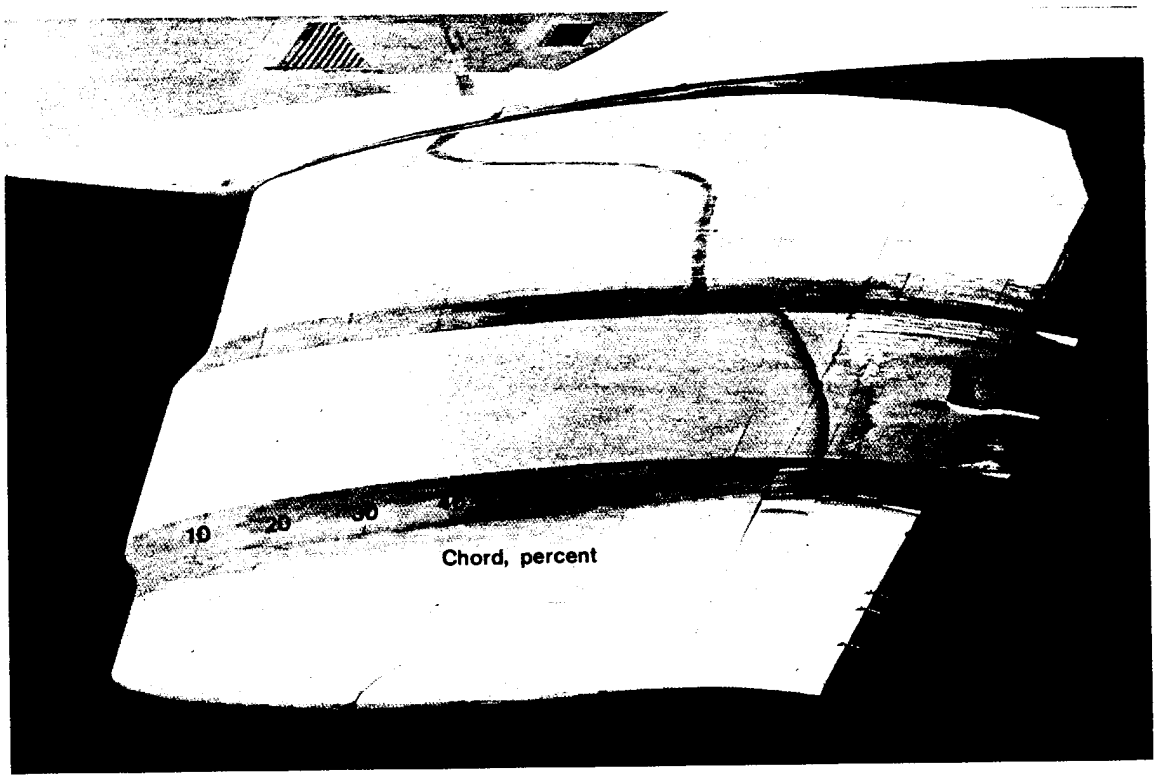

ECN 13425

(b) Test section with oil.

Figure 11. In-flight oil-flow photograph and upper surface distribution on airfoil test section at M = 0.82, α = 4.8°, and Λ = 9°.

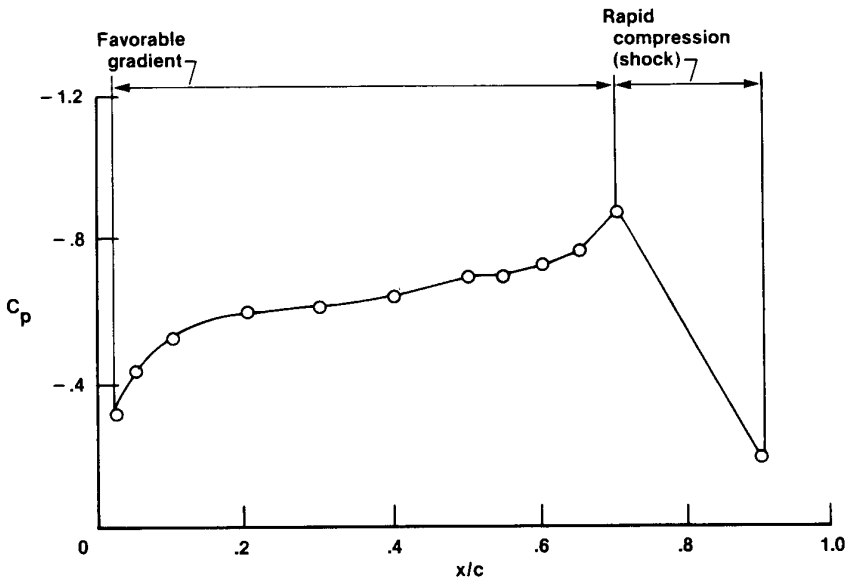

(a) Pressure distribution for flight data with oil.

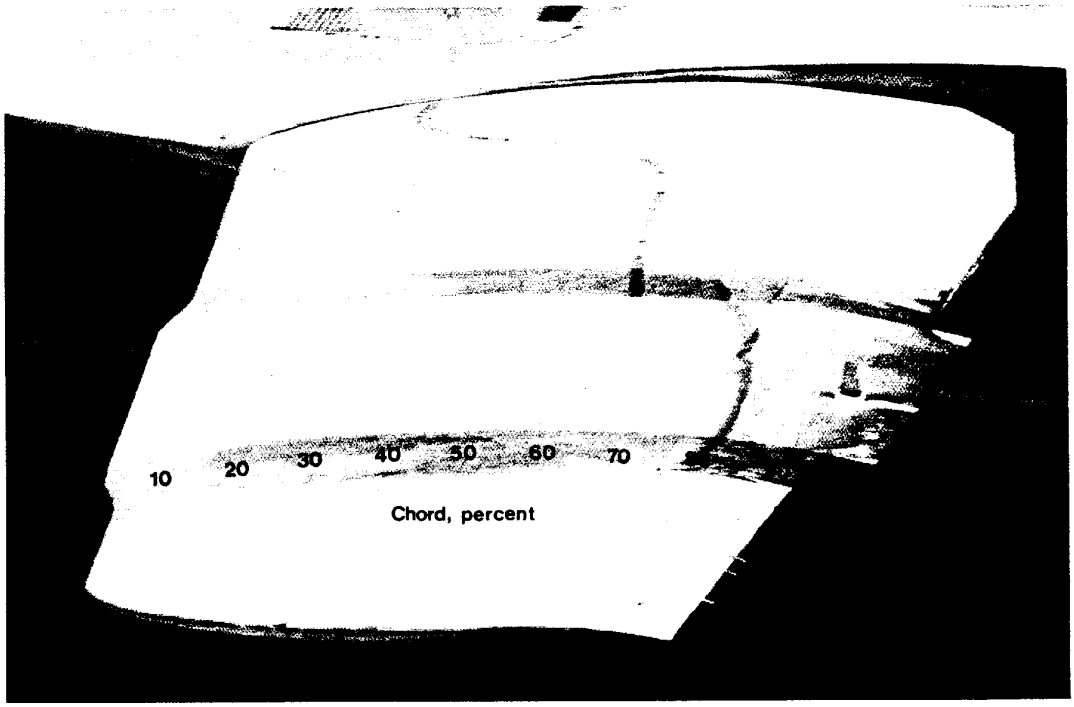

ECN 13426

(b) Test section with oil.

Figure 12. In-flight oil-flow photograph and upper surface distribution on airfoil test section at M = 0.83, α = 5.0°, and Λ = 9°.

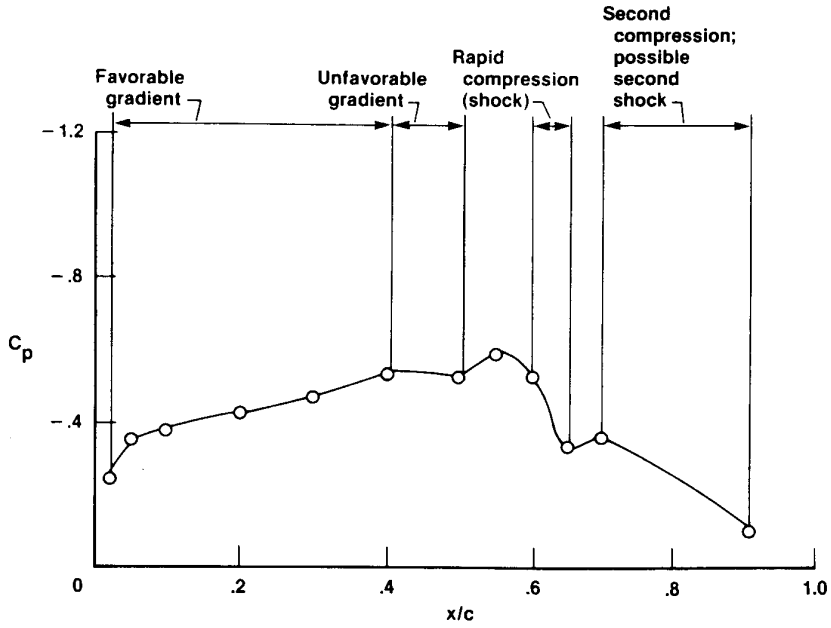

(a) Pressure distribution for flight data with oil.

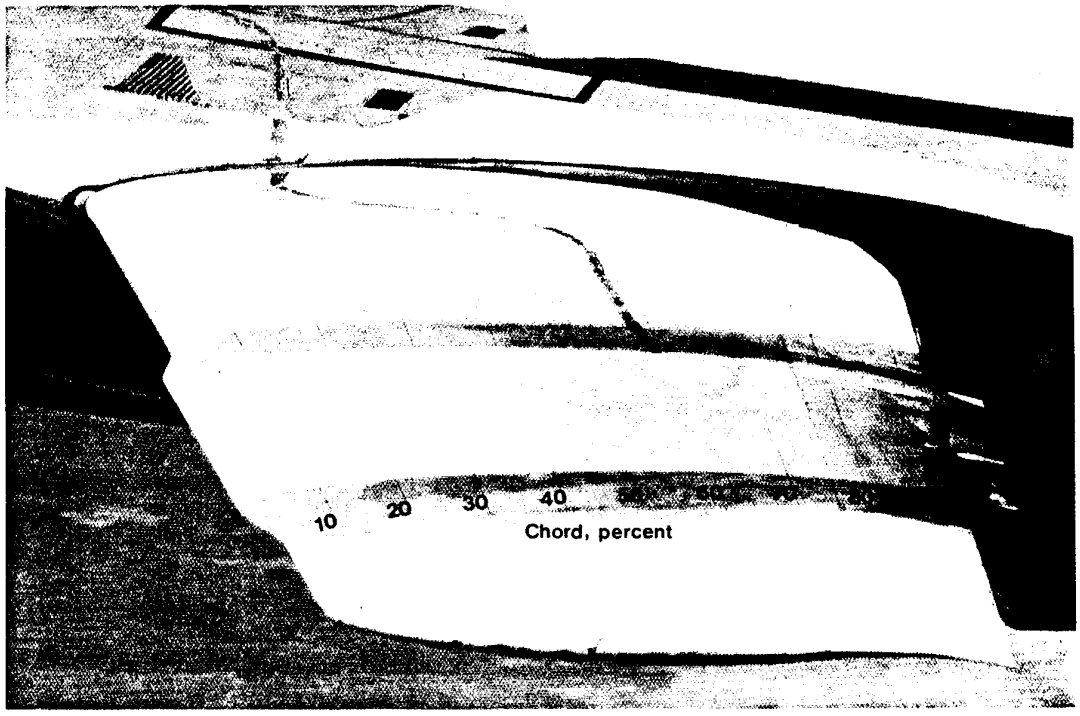

ECN 13430

(b) Test section with oil.

Figure 13. In-flight oil-flow photograph and upper surface distribution on airfoil test section at M = 0.85, α = 4.1°, and Λ = 25°.

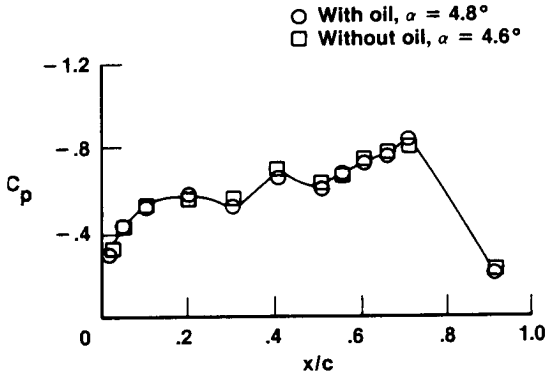

(a) $M = 0.82$, $\Lambda = 9°$.

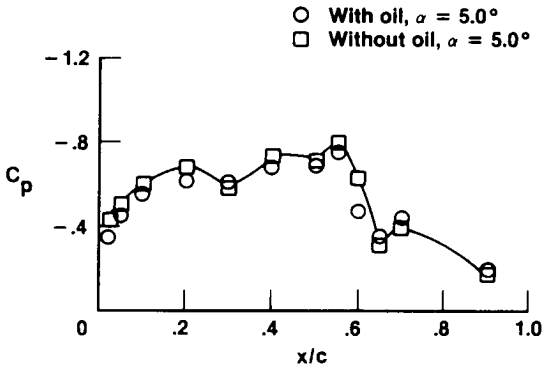

(b) $M = 0.83$, $\Lambda = 16°$.

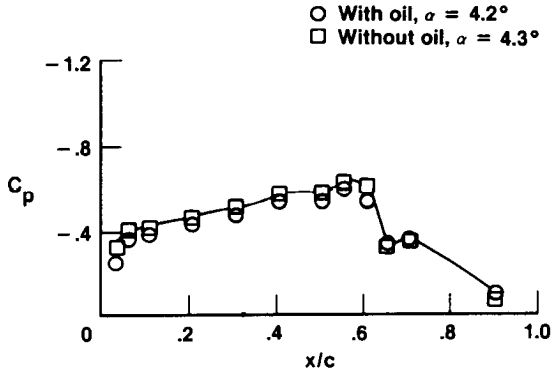

(c) $M = 0.85$, $\Lambda = 25°$.

Figure 14. Comparison of test section upper surface pressure distribution with and without oil.

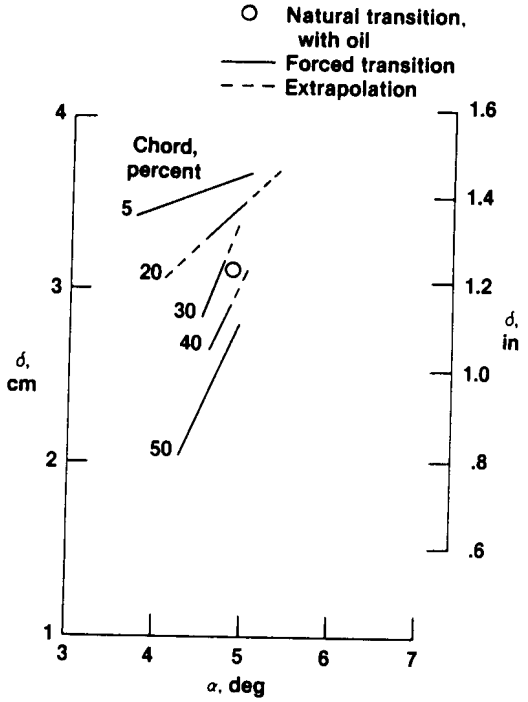

(a) $M = 0.81$, $\Lambda = 9°$.

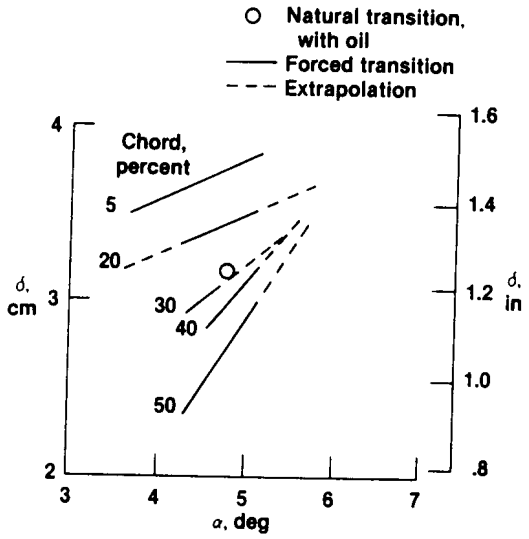

(b) $M = 0.82$, $\Lambda = 9°$.

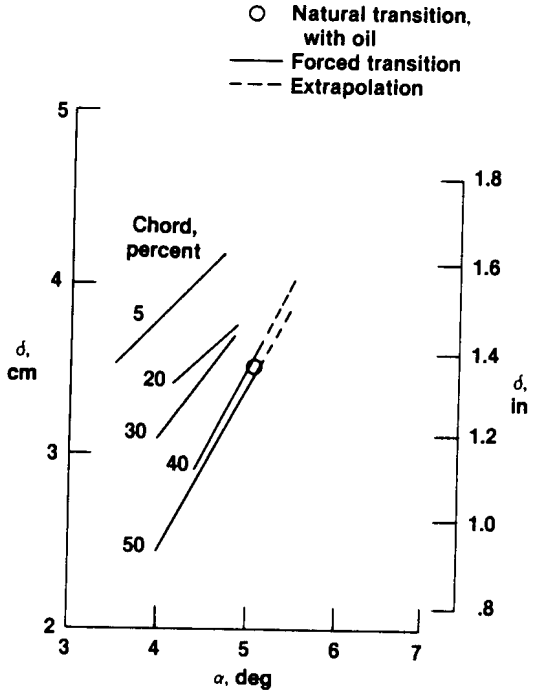

(c) $M = 0.83$, $\Lambda = 9°$.

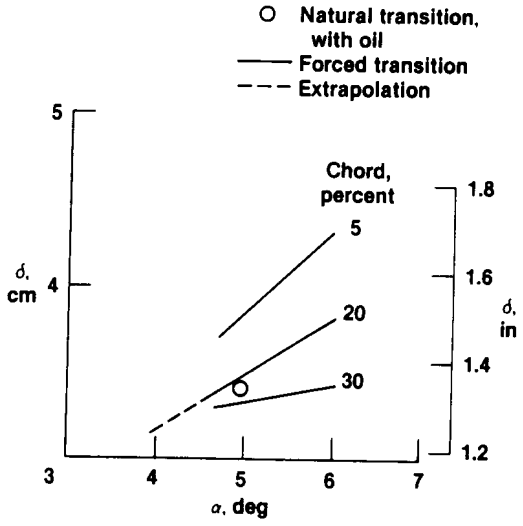

(d) $M = 0.83$, $\Lambda = 16°$.

Figure 15. Variation of boundary-layer thickness with angle of attack for various forced transition locations and natural transition.

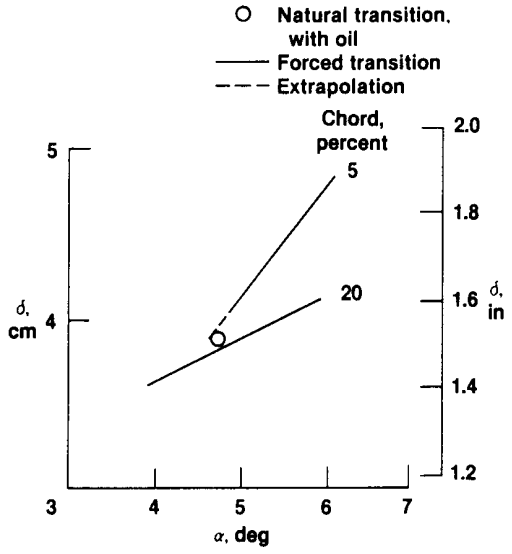

(e) $M = 0.85$, $\Lambda = 25°$.

Figure 15. Concluded.

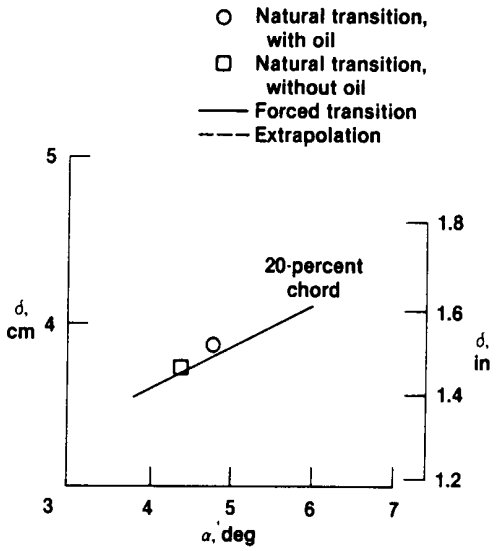

Figure 16. Variation of boundary-layer thickness with angle of attack for natural transition with and without oil, $M = 0.85$ and $\Lambda = 25°$.

1. Report No.	2. Government Accession No.	3. Recipient's Catalog No.
NASA TP-2395		

4. Title and Subtitle	5. Report Date
In-Flight Surface Oil-Flow Photographs With Comparisons to Pressure Distribution and Boundary-Layer Data	April 1985
	6. Performing Organization Code
7. Author(s)	8. Performing Organization Report No.
Robert R. Meyer, Jr., and Lisa A. Jennett	H-1184
	10. Work Unit No.
9. Performing Organization Name and Address	11. Contract or Grant No.
NASA Ames Research Center Dryden Flight Research Facility P.O. Box 273 Edwards, California 93523	
12. Sponsoring Agency Name and Address	13. Type of Report and Period Covered
National Aeronautics and Space Administration Washington, D.C. 20546	Technical Paper
	14. Sponsoring Agency Code
	RTOP 505-31-21

15. Supplementary Notes

16. Abstract

Upper surface oil-flow photographs were obtained at transonic speeds on an F-111 transonic aircraft technology (TACT) aircraft, which had been fitted with a natural laminar-flow airfoil section. The oil-flow photographs were interpreted with regard to shock and boundary-layer characteristics and compared to results obtained from pressure distributions and boundary-layer measurements. Results indicated that flow phenomena (such as shock location and strength) and chord location of boundary-layer characteristics (such as transition location) could be correctly identified from the oil-flow photographs.

17. Key Words (Suggested by Author(s))	18. Distribution Statement
In-flight flow visualization In-flight oil-flow visualization Pressure distribution Boundary-layer measurements	FEDD distribution STAR category 02

19. Security Classif. (of this report)	20. Security Classif. (of this page)	21. No. of Pages	22. Price
Unclassified	Unclassified	26	

Available through NASA's Industrial Applications Centers.